LOS Ground Displacement Monitoring in Northeast Tunisia Using SBAS InSAR

Imen Brini, Denis Feurer, Riadh Tebourbi, Fabrice Vinatier, Riadh Abdelfattah

LOS Ground Displacement Monitoring in Northeast Tunisia Using SBAS InSAR

Imen Brini[1,2], Denis Feurer[1], Riadh Tebourbi[2], Fabrice Vinatier[1], and Riadh Abdelfattah[2]

[1] UMR LISAH, Univ. Montpellier, AgroParisTech, INRAE, IRD, Institut Agro Montpellier, Montpellier, France
[2] Higher School of Communications of Tunis COSIM Lab, University of Carthage, Tunis, Tunisia
imen.brini@ird.fr

Abstract. The Lebna watershed in northeast Tunisia is marked by its important agricultural activities and its hydro-geological settings, enhancing its susceptibility to various geohazards including land subsidence and uplift. This study monitors the Line of Sight (LOS) deformation through the Interferometric Synthetic Aperture Radar (InSAR) technique. The main observations are LOS velocity maps derived from the Small Baseline Subset - InSAR, which were calculated from ESA Sentinel-1 satellites for the period 2015-2023. The SAR data resulted in velocities ranging between -1.05 and $+0.80$ cm/year. Both subsidence and uplifting trends were observed in different areas, indicating that the ground deformations in the study region could be dependent on geological and hydrogeological factors.

Keywords: SAR · radar interferometry · InSAR · SBAS · Sentinel-1 · ground displacement

1 Introduction

Ground displacement is a gradual or sudden movement of the Earth's surface, mainly caused by natural phenomena such as drought and flood inundation especially under climate change conditions, or excessive human intervention, such as groundwater over-pumping and urban construction.

Beyond these drivers, several mechanisms can intensify the extent and variability of ground deformation. Long-term consolidation of soft alluvial deposits contributes to slow but persistent subsidence [16]. In agricultural areas, the ground water over-pumping of irrigation purposes has been identified as a key factor of land subsidence [1]. Such effects are often more pronounced in areas with intensive farming practices and limited water regulation. The precipitation also plays a critical role in shaping ground displacement dynamics [22, 2].

Over the past few decades, observation methods to monitor ground displacement have been widely developed. Commonly, terrestrial approaches such as leveling and GPS surveys [20] at several measurement points provide high precision,

but are applied in small coverage areas, as they are costly and time-consuming [19].

Recently, satellite remote sensing technologies, specifically the synthetic aperture radar interferometry (InSAR) technology has been used for ground displacement monitoring. This technology is based on the principle of using the phase difference of at least two high-resolution complex SAR images acquired from different orbit positions and/or different time.

For long-term ground displacement monitoring, time-series InSAR technology based on multi-temporal series of images has been investigated. This technology significantly reduces atmospheric effects and time-space decoherence that influence the reliability of InSAR monitoring. The time-series InSAR technology is mainly represented by the permanent scatterer synthetic aperture radar interferometry (PS-InSAR) [10] and the small baseline subset synthetic aperture radar interferometry (SBAS-InSAR) [5, 17].

The PS-InSAR approach is based on determining stable reflectors in the multi-temporal interferometric SAR images, which are the permanent scatterers (PS). Ferretti et al. [10] proposed an amplitude dispersion index to determine the PS. Typically, PS can be artificial structures or natural objects, such as uncovered rocks, that have a stable signal phase from different acquisitions, showing a high coherence over a SAR data stack [15]. The SBAS-InSAR approach relies on coherent interferograms with a small geometric and temporal baseline to maintain coherence over distributed scatterers [10].

Although the PS approach is more suitable for studying infrastructure behavior because of its focus on stable, point-like reflectors, the SBAS approach is better suited for monitoring long-term geological patterns, as it captures the behavior of distributed scatterers over time. Using the SBAS approach, temporal variations of the Line of Sight (LOS) signal and time-series accumulated displacement can be generated [3].

In this context, one of the most used tools is Sentinel-1 imagery, known for its frequent revisit times, large spatial coverage, all-weather monitoring capabilities due to its active imaging mode, and open access datasets. Consequently, Sentinel-1 imagery has been used in several research fields for monitoring ground displacement.

Yastika et al. [21] explored land subsidence in the coastal city of Semarang in Indonesia for different periods and sensors, including Sentinel-1. They used SBAS technique, and found a high correlation with sediments that subside due to natural consolidation.

For instance, Cigna and Tapete [8] employed the Parallel Small Baseline Subset (P-SBAS) to process Sentinel-1 data SAR images acquired from 2014 to 2020 over a coastal study area in southern Italy. LOS velocity ranged from -3.7 to $+1.6$ cm/year in the ascending dataset, and between -2.0 and $+1.9$ cm/year in the descending dataset exhibiting the precision of the deformation products derived from P-SBAS processing.

Similarly, Abdelfattah [2] used the P-SBAS to process Sentinel-1 data SAR images acquired in two successive periods, 2018-2019 and 2021-2022, covering

the Cap Bon peninsula in northeastern Tunisia. The maximum subsidence rate reaches −19.62 cm/year and was explained by the over-exploitation of groundwater during dry periods.

Zhou et al. [23] processed Sentinel-1 image acquired from 2019 to 2022 covering the Hangjiahu plain in China with SBAS-InSAR approach. The annual average deformation velocity ranged from −21.0 mm/year to +11.9 mm/year. The spatial distribution of the deformation velocity is relatively uneven, with significant subsidence in local areas reaching a maximum subsidence of −85.8 mm.

Overall, InSAR demonstrated to be relevant for ground displacement assessment in different geoscience applications. Accordingly, the main aim of this research is to analyze and detail the surface ground movements in the Lebna watershed in Cap Bon peninsula in Tunisia. This analysis is conducted through an SBAS approach, using synthetic aperture radar (SAR) data. The SAR images, provided by the Sentinel-1 satellites of the Copernicus Program, cover a period from 24 November 2015 to 02 August 2023. The extended temporal coverage enhances InSAR signal coherence and phase stability. This enables more robust P-SBAS processing and reliable detection of both gradual and rapid ground deformation trends over time.

This study focuses on extracting and interpreting the relevant surface deformation from these satellite observations to gain a deeper understanding of the Lebna watershed surface dynamics during this period, as it plays a key role in regional agriculture and water resources.

The paper is structured as follows. First, a brief description of the study area, the dataset, and the SBAS-InSAR technique is provided, and the proposed monitoring methodology is thoroughly presented in Section 2. The main findings are reported in Section 3 and discussed in Section 4, followed by the conclusion in Section 5.

2 Material and methods

2.1 Study area

The Lebna watershed is located in the eastern coastal plain in northeastern Tunisia, in the Cap Bon peninsula. It has an area of 210 km^2 approximately. The watershed is bordered on the northwest by Djebel Sidi Abderrahmane, that reaches elevations of 650 m above sea level, to the northwest by the Menzel Temime town, to the southwest by the Tafelloune town, and to the southeast by a slightly marked relief, occupied mainly by annual crops and orchards at elevations around sea level.

The study area is characterized by a typical Mediterranean climate, with hot, dry summers and cool, cold winters. The climate effects vary spatially and temporally, from a rainy regime at the top of the Djebel in the northwest, with more than 700 mm/year, to a semi-arid climate in the southeast, with less than 500 mm/year [18]. The rainy season starts at the end of September and lasts

through February with moderate rain. The evaporative demand is almost 1200 mm. In the summer, the highest temperature can reach 45 °C [12].

The watershed is an agricultural region with intense plant production, including fruit culture, field crops, pastures, and olive cultivation [12]. In fact, around 34% of the watershed area is covered by natural vegetation (forests, shrubs, pastures, etc.). Annual crop, including grain cereals, fodder crops, spices, and legumes, cover about 49% of the watershed area. Perennial crops, mainly olive trees, cover 8% of the total area of the watershed [18].

In the Cap Bon peninsula, the Abderrahmane belt is the most prominent tectonic feature. The foreland basins of Dakhla and Takelsa extend in a NE–SW direction, roughly paralleling the deformational front of the Abderrahmane anticline. Faults trending north and northwest controlled the drainage patterns of the Cap Bon peninsula [14]. Geologically, the outcrops of Lebna plain are represented by Miocene-Pliocene-Quaternary sediments [24]. Figure 1 represents the geological setting of the Cap Bon peninsula.

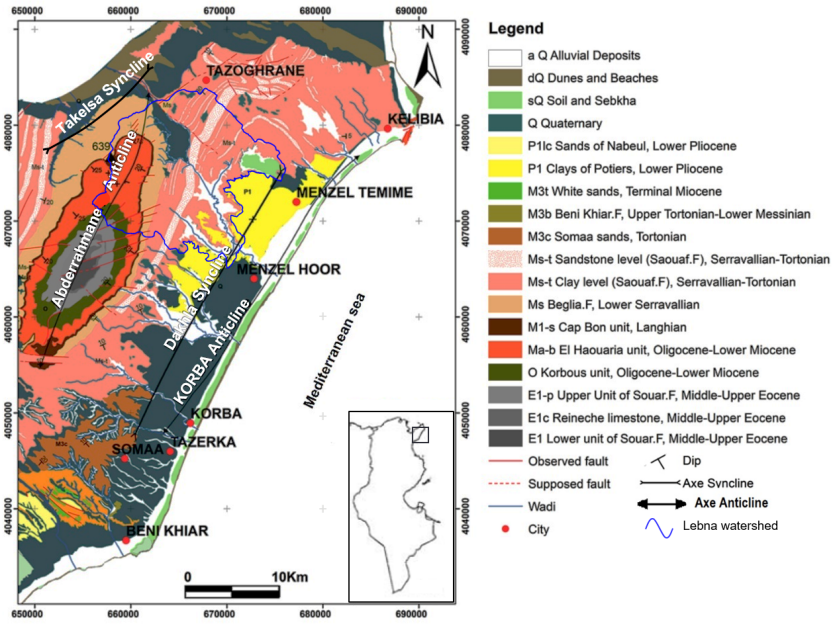

Fig. 1. Geological map of the Cap Bon peninsula, northeastern Tunisia. Adapted from [4].

The Lebna aquifer is included in the costal aquifer in the northeast of the Cap Bon peninsula. The latter is surrouneded by Djebel Sidi Abderrahmane in the west, Kelibia city in the north, the Mediterranean Sea in the east and the Beni Khiar region in the south. It is tapped by 9239 wells, where 2.5% of them are

equipped with irrigation pumps. Since the early 1960s, population growth and the shortage of surface water have led to the over-exploitation of groundwater in the Cap Bon region, mainly for tap water and irrigation purposes [24].

Consequently, all these factors, including climatic variability, geological structures, and the over-exploitation of groundwater, render the region susceptible to various geohazards and contribute to ground deformation, particularly in hotspots of groundwater pumping for local agricultural activities [1, 2].

2.2 Interferometric SAR data processing

A total of 208 Sentinel-1 SAR scenes were used for interferometric analysis. The Single Look Complex (SLC) processing level (L-1) SAR images were acquired with Sentinel-1A and Sentinel-1B satellites in right-looking mode along the descending track T95, covering the period between 24 November 2015 and 02 August 2023.

The SAR images were acquired in the Interferometric Wide (IW) swath mode with the vertical-vertical (VV) polarization. The ground range and azimuth resolution is 5 m and 20 m, respectively. They were supplied by the ESA (European Space Agency) through the Geohazards Exploitation Platform (GEP) [11].

The multi-interferogram processing was performed in ESA's GEP using the "P-SBAS Sentinel-1" service v.1.8.1 within the "Area monitoring services " Thematic App. The processing approach is based on the SBAS technique [5], which has been optimized by parallel computing to efficiently run on high-performance distributed-computing infrastructure [7, 9].

The principle of the SBAS technique consists in selecting satellite image pairs that exhibit both a small perpendicular baseline, defined as the distance between the position of two acquisition points of the satellite sensor along his orbital track, and a small temporal baseline, which corresponds to the time interval between the acquisition of the two images, and obtaining the phase difference between the images in the differential interferograms.

The small perpendicular and temporal baseline pairs selected to form the interferograms enable the reduction of the noise effects on the multi-temporal series of differential interferograms and optimize the number of measurement points detected on earth.

The topographic phase components were derived and subtracted based on the 1 arcsec resolution Shuttle Radar Topography Mission digital surface model provided by NASA. The interferograms were then noise-filtered using the Goldstein filter with 0.5 weight, and a threshold on the minimum allowed temporal coherence is fixed at 0.75 to select coherent target points. Additionally, the atmospheric phase components were identified and removed.

The Multi-Temporal Analysis processing mode was selected to derive mean LOS velocity in cm/year and date-by-date displacement time series for each coherent target point spatially georeferenced by longitude, latitude, and altitude. Particularly, the displacement measures are not absolute values, as these values are relative to a specific point, known as a reference point, defined within a stable and coherent area [6]. The reference point for the descending P-SBAS processing

was set at 36°45'30.3"N 10°58'36.1"E, indicated in figure 2 by a black star, and the mean LOS velocity values and time series were referenced accordingly.

2.3 Points selection

In order to explore the temporal evolution of ground deformation, displacement time-series profiles were extracted for selected coherent target points identified through interferometric analysis. These profiles provide detailed insight into how ground displacement varies over time, enabling a better understanding of both the magnitude and behavior of land surface movements across the study area.

A total of 12 representative coherent target points were selected for this analysis, based on their mean velocity of LOS displacement throughout the full observation period. Specifically, four points correspond to areas exhibiting the highest negative mean velocity of LOS displacement, indicative of significant subsidence, while four other points display the highest positive mean velocity of LOS displacement, representing areas of uplift. Additionally, four points with mean velocity of LOS displacement approaching zero were chosen to characterize areas of minimal displacement and stable ground conditions. This selection strategy enables a comparative analysis of contrasting deformation trends, subsidence and uplift, while also incorporating stable points.

3 Results

The coherent target points are mainly dense on natural vegetation lands and urbanized areas (Fig. 2). However, in annual crops and orchards, coherent target points are sparse because of the loss of temporal coherence. Seasonal planting, harvesting, and crop rotation disrupt the surface, causing rapid changes in radar backscatter.

The processed area is shown in figure 2(a). The velocity of displacements along LOS ranges from -1.05 to $+0.80$ cm/year. Negative values denote a displacement away from the satellite sensor along the LOS, suggesting a subsidence of the ground surface. However, positive values denote a displacement toward the satellite sensor along the LOS, suggesting an uplift of the ground surface. The mean velocity value is $+0.02$ cm/year, with a standard deviation of 0.18 cm/year. Although the mean velocity value suggests a minimal net change, the standard deviation exhibits significant spatial variability in the displacement velocity, indicating that the displacement pattern is not uniform across the entire study area.

The displacement history of 12 coherent target points through their LOS time-series at the 208 dates of the overall observation period is shown in figure 3. The coherent target points were selected according to their mean velocity of LOS displacement. Points P1, P2, P3, and P4 recorded the maximum mean velocity of LOS displacement, and points P5, P6, P7, and P8 recorded the minimum mean velocity of LOS displacement. The points P9, P10, P11, and P12 are points with a mean velocity of LOS displacement approaching zero, suggesting stable points.

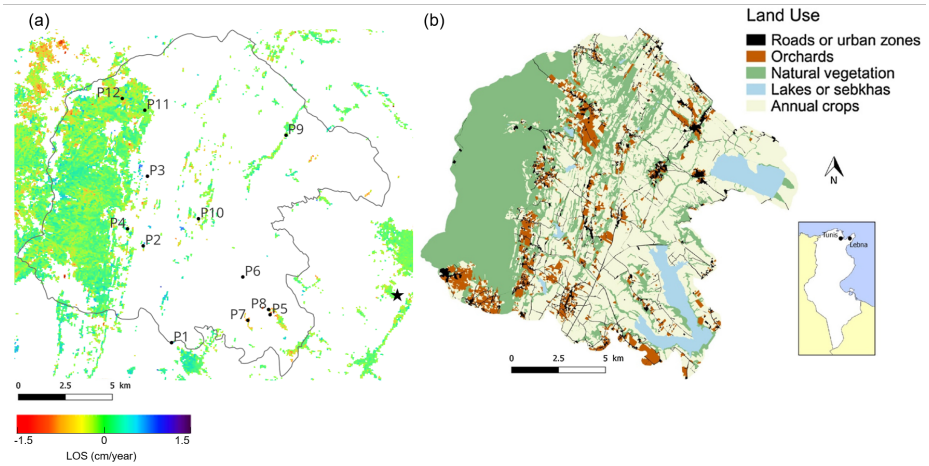

Fig. 2. (a) Mean velocity of LOS displacement map (2015-2023) and (b) land use map [18] of the Lebna watershed. The black star in (a) is the reference point, and the black line outlines the extent of the Lebna watershed.

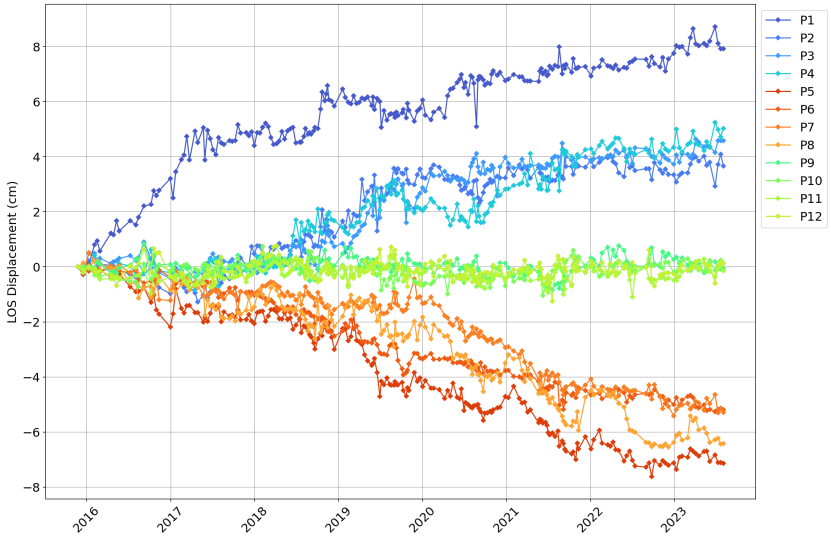

Fig. 3. LOS displacement time-series.

The displacement of point P1 reaches the maximum uplift of +8.72 cm, with a mean velocity of LOS displacement of +0.80 cm/year. This indicates a consistent and significant upward movement in this point over the observation period. The points P2, P3 and P4 exhibit relative stability until almost mid-2018, and then an uplift is observed. This could be indicative of a response to external influences

or a natural shift in the dynamics of the area, which might require a detailed inspection to identify the specific cause. These points are experiencing the same trend, suggesting that the area surrounding these points might be undergoing similar processes.

In contrast, points P5, P6, P7 and P8 show the same subsiding trend with a mean velocity of LOS displacement of around −1 cm/year. This negative displacement suggests a slow but steady downward movement, likely due to subsidence processes. The maximum subsidence reaches −7.61 cm for point P5.

Lastly, the points P9, P10, P11 and P12 are almost stable points with a mean velocity of LOS displacement of +0.0001 cm/year. These points are experiencing negligible movement, suggesting that they are located in regions of high stability, where no significant environmental or human influences are causing ground displacement.

It is worth mentioning that the amount of the total displacement, whether positively or negatively, reflects the clear distinction between the uplifted areas, the subsiding areas, and the more stable ones. Nevertheless, this evidence is related to the reference point located in an urbanized area area, indicated by the black star in figure 2. Consequently, any deformation signal is spatially relative to this point, and temporally relative to the image acquired in 24 November 2015.

4 Discussion

The ground surface displacement is linked to natural and anthropogenic events characterizing the study area. For instance, land subsidence is mainly located in the neighboring areas of ground water over-exploitation [1, 2] and in areas highly susceptible to soil erosion [13]. For the points P5, P6, P7 and P8, the observed subsidence could be attributed to their proximity to the riverbanks, where subsidence tends to be more pronounced compared to areas farther away from the river.

In contrast, uplift patterns could be associated with natural geodynamic processes. The neotectonic activity resulted in gradual uplift processes, mainly in the Abderrahmane area that experienced the switch from Late Miocene crustal extension to post-Tortonian to Quaternary compressional tectonics [14]. Additionally, uplift can also be observed in urbanized areas as well as in agricultural regions dominated by annual crops or orchards. In these cases, uplift may be linked not only to anthropogenic influences, such as infrastructure development and land use changes, but also to natural processes related to soil moisture dynamics and subsurface fluid flow.

The predominance of stability is commonly due to flat topography, which makes them less susceptible to surface ground displacement compared to steeper and more geodynamically active zones.

In addition, precipitation is a key factor that can trigger ground deformation with varying degrees of effects, especially on surface subsidence. To explore the relationship between rainfall and surface deformation, the subsided points are

plotted along with the precipitation rates that were collected and averaged from seven rain gauge stations in the study area and accumulated monthly (Fig. 4).

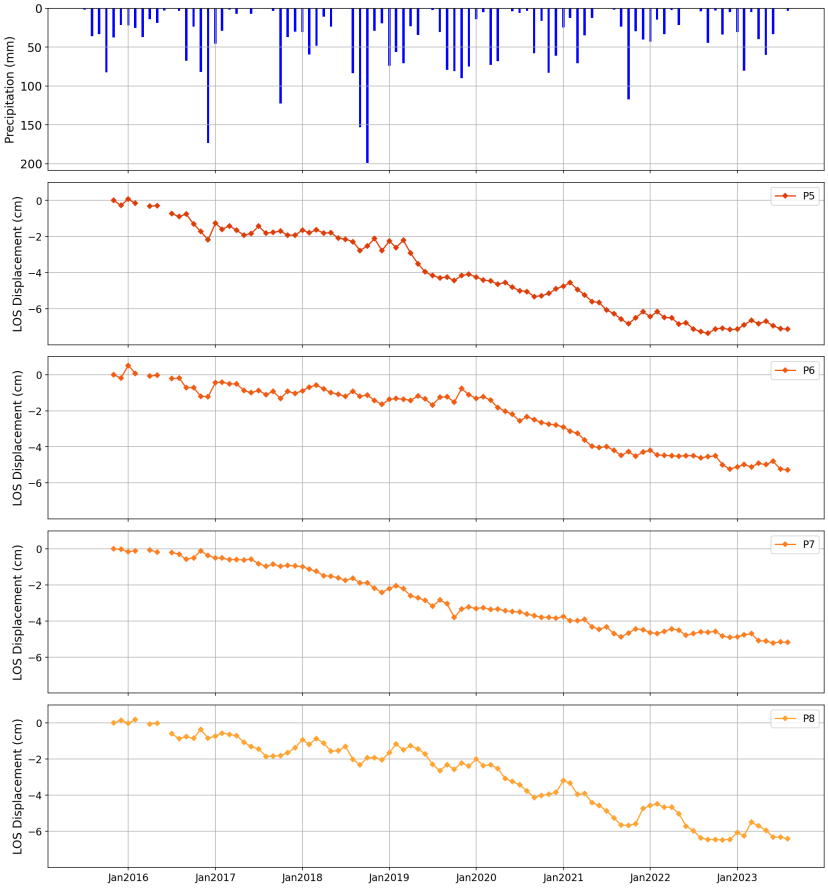

Fig. 4. Mean LOS displacement with monthly accumulated precipitation.

The rainy season begins at the end of September and continues until February, with moderate rainfall throughout. This period has the highest continuous precipitation of the year, which accounts for approximately 70% of annual precipitation. Consequently, the impact of rainfall on surface deformation is significant. In contrast, summer experiences extremely low rainfall, with a mean of less than 1 mm, indicating a dry period.

The higher precipitation peaks in the rainy season of each year affect the ground displacement. The increase in precipitation leads to a higher groundwater recharge, which diminishes the effect of pumping on land deformation. During the dry season, the LOS displacement becomes more pronounced than

during the wet period. These patterns are more evident for the point P8, but less noticeable for the point P5. Although these points are relatively close to each other and situated near the riverbanks, where subsidence typically intensifies due to sediment instability, the LOS displacement remains variable in these locations. This variability can be attributed to differences in soil texture and composition (Fig. 1).

For the point P6, a pronounced subsidence is observed starting from the beginning of 2020. This deformation is unlikely to be directly related to precipitation, as earlier and heavier rainfall events (end of 2017 and 2018, respectively) did not result in significant displacement. Instead, the observed subsidence can be attributed to changes in land use or anthropogenic activities.

The LOS displacement for the point P7 shows a gradual and continuous decrease over time. This behavior does not appear to be correlated with rainfall patterns, suggesting that the displacement could be driven by other factors.

Additionally, the LOS displacement can be attributed to the agro-system gradient observed along the upstream-downstream transect of the watershed, transitioning from extensive rainfed agriculture to intensive irrigated systems. The intensification of irrigation practices in the downstream areas is likely to increase groundwater extraction, which can enhance subsidence in localized zones.

Therefore, while precipitation may significantly influence the land deformation in certain areas, it is not the exclusive controlling factor, and the impact of soil characteristics, land use, and human activities must also be considered.

It is worth mentioning that approximately 49% of the study area is covered by annual crops, which significantly limits the density of coherent points due to temporal decorrelation mainly caused by seasonal planting and harvesting. This lack of coherent targets in such regions limits the achievement of high-resolution displacement mapping across the entire watershed. Consequently, the ground displacement dynamics within the annual crop zones remain largely unknown, representing a gap in spatial coverage.

5 Conclusion

The time-series analysis of Sentinel-1 satellite data was performed to study ground deformation in the Lebna watershed, from 2015 to 2023. Multi-temporal interferometry using SBAS technique was processed with GEP resulting in LOS velocity map.

This study provides significant advancements in understanding ground surface dynamics in the Lebna watershed. While some areas experienced a subsidence reaching −7.61 cm, other areas recorded an uplift of more than +8 cm. These deformations are closely related to factors such as land use, geological context, and variations in precipitation, which together influence the magnitude of ground displacement across the watershed. The correlation between precipitation data and ground deformation suggests that hydrological factors influence the ground displacement.

The interactions between human activities, geodynamic processes, and climate variability trigger ground displacement in the Lebna watershed. Monitoring the deformation trends and velocities is essential for future land management and disaster risk mitigation strategies in the Lebna watershed.

Acknowledgments. This publication was made possible through support provided by the IRD.
This work has been supported by the Programme National de Télédétection Spatiale (PNTS, grant N° PNTS-2023-05).

Disclosure of Interests. The authors declare that there are no potential conflicts of interest that could have influenced the objectivity of this research or the writing of this paper.

References

1. Abdelfattah, R.: Land Subsidence and Surface Water Extent Relationship Assessment Using Sentinel 1 & 2 Data in the Cap-Bon Peninsula in Tunisia. In: IGARSS 2023-2023 IEEE International Geoscience and Remote Sensing Symposium. pp. 2866–2869. IEEE (2023)
2. Abdelfattah, R.: Exploring the Relationship between Land Subsidence and Precipitation in the Lebna Watershed in Tunisia Using SBAS-InSAR Analysis. In: IGARSS 2024-2024 IEEE International Geoscience and Remote Sensing Symposium. pp. 5386–5389. IEEE (2024)
3. Anjasmara, I.M., Yulyta, S.A., Taufik, M.: Application of time series InSAR (SBAS) method using sentinel-1A data for land subsidence detection in Surabaya city. International Journal on Advanced Science, Engineering and Information Technology **10**(1), 191–197 (2020)
4. Bellali, A., Horriche, F.J., Gabtni, H., Bédir, M.: Seismic reflection and structuring characterization of deep aquifer system in the Dakhla syncline (Cap Bon, North-Eastern Tunisia). Journal of African Earth Sciences **140**, 134–150 (2018)
5. Berardino, P., Fornaro, G., Lanari, R., Sansosti, E.: A new algorithm for surface deformation monitoring based on small baseline differential SAR interferograms. IEEE Transactions on geoscience and remote sensing **40**(11), 2375–2383 (2002)
6. Bonaldo, G., Caprino, A., Lorenzoni, F., da Porto, F.: Monitoring displacements and damage detection through satellite MT-INSAR techniques: A new methodology and application to a case study in rome (Italy). Remote Sensing **15**(5), 1177 (2023)
7. Casu, F., Elefante, S., Imperatore, P., Zinno, I., Manunta, M., De Luca, C., Lanari, R.: SBAS-DInSAR parallel processing for deformation time-series computation. IEEE Journal of Selected Topics in Applied Earth Observations and Remote Sensing **7**(8), 3285–3296 (2014)
8. Cigna, F., Tapete, D.: Sentinel-1 big data processing with P-SBAS InSAR in the geohazards exploitation platform: An experiment on coastal land subsidence and landslides in Italy. Remote Sensing **13**(5), 885 (2021)

9. De Luca, C., Bonano, M., Casu, F., Manunta, M., Manzo, M., Onorato, G., Zinno, I., Lanari, R.: The parallel SBAS-DInSAR processing chain for the generation of national scale sentinel-1 deformation time-series. Procedia computer science **138**, 326–331 (2018)
10. Ferretti, A., Prati, C., Rocca, F.: Permanent scatterers in SAR interferometry. IEEE Transactions on geoscience and remote sensing **39**(1), 8–20 (2002)
11. Galve, J.P., Pérez-Peña, J.V., Azañón, J.M., Closson, D., Caló, F., Reyes-Carmona, C., Jabaloy, A., Ruano, P., Mateos, R.M., Notti, D., et al.: Evaluation of the SBAS InSAR service of the European space Agency's Geohazard Exploitation Platform (GEP). Remote Sensing **9**(12), 1291 (2017)
12. Gasmi, A., Gomez, C., Chehbouni, A., Dhiba, D., Elfil, H.: Satellite multi-sensor data fusion for soil clay mapping based on the spectral index and spectral bands approaches. Remote Sensing **14**(5), 1103 (2022)
13. Gaubi, I., Chaabani, A., Ben Mammou, A., Hamza, M.: A GIS-based soil erosion prediction using the revised universal soil loss equation (RUSLE)(Lebna watershed, Cap Bon, Tunisia). Natural Hazards **86**, 219–239 (2017)
14. Ghribi, R., Affouri, H., Bouaziz, S.: Tectonic inversion of Late Miocene extensional deformations in northeastern Tunisia (Cap Bon Peninsula-Sahel area). Geologica Carpathica **74**(3), 261–277 (2023)
15. Hu, B., Chen, J., Zhang, X.: Monitoring the land subsidence area in a coastal urban area with InSAR and GNSS. Sensors **19**(14), 3181 (2019)
16. Jiang, H., Balz, T., Cigna, F., Tapete, D.: Land subsidence in Wuhan revealed using a non-linear PSInSAR approach with long time series of COSMO-SkyMed SAR data. Remote Sensing **13**(7), 1256 (2021)
17. Lanari, R., Mora, O., Manunta, M., Mallorquí, J.J., Berardino, P., Sansosti, E.: A small-baseline approach for investigating deformations on full-resolution differential SAR interferograms. IEEE transactions on geoscience and remote sensing **42**(7), 1377–1386 (2004)
18. Mekki, I., Bailly, J.S., Jacob, F., Chebbi, H., Ajmi, T., Blanca, Y., Zairi, A., Biarnès, A.: Impact of farmland fragmentation on rainfed crop allocation in Mediterranean landscapes: A case study of the Lebna watershed in Cap Bon, Tunisia. Land use policy **75**, 772–783 (2018)
19. Raspini, F., Caleca, F., Del Soldato, M., Festa, D., Confuorto, P., Bianchini, S.: Review of satellite radar interferometry for subsidence analysis. Earth-Science Reviews **235**, 104239 (2022)
20. Rózsa, S., Heck, B., Mayer, M., Seitz, K., Westerhaus, M., Zippelt, K.: Determination of displacements in the upper Rhine graben Area from GPS and leveling data. International Journal of Earth Sciences **94**, 538–549 (2005)
21. Yastika, P., Shimizu, N., Abidin, H.: Monitoring of long-term land subsidence from 2003 to 2017 in coastal area of Semarang, Indonesia by SBAS DInSAR analyses using Envisat-ASAR, ALOS-PALSAR, and Sentinel-1A SAR data. Advances in Space Research **63**(5), 1719–1736 (2019)
22. Zhang, M., Pan, J., Ma, P., Lin, H.: Identification and Analysis on Surface Deformation in the Urban Area of Nanchang Based on PS-InSAR Method. Remote Sensing **17**(1), 157 (2025)
23. Zhou, L., Wei, B., Chen, G., Liu, S., Li, X., Luo, Z., Qin, D., Zhang, D.: Insar time series analysis of natural and anthropogenic coastal plain subsidence: A case of hangjiahu plain. Geodesy and Geodynamics (2024)
24. Ziadi, A., Hariga, N.T., Tarhouni, J.: Mineralization and pollution sources in the coastal aquifer of Lebna, Cap Bon, Tunisia. Journal of African Earth Sciences **151**, 391–402 (2019)